

## High-resolution remote sensing of intertidal ecosystems: A low-cost technique to link scale-dependent patterns and processes

Frédéric Guichard<sup>1</sup> and Edwin Bourget

GIROQ, Département de biologie, Pavillon Vachon, Université Laval, Québec Qc G1K7P4 Canada

Jean-Paul Agnard

Département des sciences géomatiques, Université Laval, Québec Qc G1K7P4 Canada

### Abstract

Linking experimentally tested local processes to natural patterns in intertidal ecosystems requires data-acquisition techniques that provide spatiotemporal data from the scale of local processes to the scale of patterns. We developed a low-cost, high-resolution remote-sensing technique based on the use of a 6-m helium-inflated blimp, a standard 35-mm camera, and photogrammetric numerical tools in order to acquire high-resolution data of environmental (i.e., topographic) and biological (i.e., algal biomass) variables over intertidal landscapes. The camera was calibrated for photogrammetric analysis, and overlapping color aerial photographs were taken at an altitude of 80 and 50 m. We performed stereo analysis of digitized images and numeric topographic restitution over an 18 × 18 m area with an error of 0.02 m along the Z axis. A normalized vegetation index (NDVI) from color-infrared images at 0.02-m resolution over the same area was computed. Algal biomass sampled within the photographed area allowed us to calibrate NDVI with algal biomass ( $R^2 = 0.73$ ,  $p < 0.01$ ). Aggregation analysis performed on a height above zero level, local topographic heterogeneity, and algal biomass confirmed, at the landscape level, previous local experimental evidence of a relationship between topographic heterogeneity and algal biomass increasing from scales of 0.5 to 2 m. Our method permits multiscale testing of local scale-dependent processes over a natural landscape.

Theoretical and empirical studies show that the analysis of large (i.e., regional) scale patterns must integrate processes occurring at the small (i.e., local) scale (Levin 1992). Theoretical and modeling efforts coupled to field measurements are now addressing questions about scaling rules from individual processes to regional patterns (Pacala et al. 1996). However, one major technical problem that remains is the lack of biological and physical data at spatial scales amenable to experimental studies (<0.5 m) and compatible with remote sensing. Although authors have stressed the usefulness of remote sensing as a tool for regional scale studies in ecology (Roughgarden et al. 1991), few efforts have been made to cover spatial scale gaps between remote sensing, which provides low-resolution data over large areas, and experimental approaches that give information about local processes but that are unable to provide continuous, spatially explicit data over large areas. Remote-sensing techniques that allow for high-resolution data acquisition remain too costly to be widely used, particularly in ecological studies requiring temporal monitoring.

Topography, and more precisely topographic variability, is known to influence abiotic and biotic properties in ecosys-

tems over a wide range of spatial scales, from km (Wolanski and Hammer 1988; Boose et al. 1994; Johnson and Hanson 1995) to <mm (Le Tourneux and Bourget 1988; Carpenter and Williams 1993). In intertidal marine habitats, topographic heterogeneity under the meter scale has been shown to influence hydrodynamics and benthic community structure (Cusson and Bourget 1997; Guichard and Bourget 1998). Intertidal macroalgae are influenced by topographic complexity through settlement at the millimeter scale (Johnson et al. 1994), through protection from ice scouring (Archambault and Bourget 1996), and from grazing pressure (Johnson et al. 1997) at the centimeter scale. At the meter scale, topographic heterogeneity was shown to decrease *Fucus* sp. biomass through its influence on hydrodynamic patterns.

Standard remote-sensing techniques like satellite imagery and airborne photography can be used to derive digital elevation model (DEM; Lillesand and Kiefer 1994) and terrestrial plant community classification at coarse resolutions (Bijlsma 1993; Jackson and Gaston 1994). In intertidal habitats, radiometric studies have established the relationship between macroalgae and near-infrared reflectance (Coulson et al. 1980; Ben Moussa et al. 1989); and aerial photography (Meulstee et al. 1988), multispectral sensor (Deysher 1993; Bajjouk et al. 1998), and satellite imagery (Guillaumont et al. 1993) have been used to map macroalgae in the intertidal at scales from 2 to 20 m. To our knowledge, there is still no civil remote-sensing technique available at reasonable costs to acquire topographic data at the cm scale. This is reflected by the very few studies that have used remote sensing as a tool in ecology to examine small scales (but see Goward et al. 1991 and Lobo et al. 1998).

We describe here a low-cost high-resolution remote-sensing technique that contributes to solve the problems alluded

<sup>1</sup> Corresponding author (frederic.guichard@giroq.ulaval.ca).

### Acknowledgements

We thank J.-B. Moutin for assistance in helping design the remote sensing device, Y. Sujobert for assistance on the field, and H. Lamarre for assistance during photo analysis. We also thank two anonymous reviewers for their help in improving previous versions of the manuscript. This research was supported by a FCAR scholarship to F.G. and by FCAR and NSERC grants to E.B. This is a contribution to the Groupe Interuniversitaire de Recherches Océanographiques du Québec (GIROQ).

to above. Our technique uses a helium-inflated blimp and a standard remotely controlled 35-mm camera. The technique was tested on an intertidal rocky shore and algal community. We present examples of results and the development of numerical treatments of images in order to obtain exhaustive spatially explicit data about topography and algal biomass. We then explore the multiscale relationship between topographic heterogeneity and macroalgae distribution. Our results show that topographic restitution from photographic images can be performed with satisfactory resolution and precision. Infrared photographs can provide very good spatially explicit data on algal biomass, even using simple, pixel-based analysis techniques. Spatial statistics performed on our data set revealed patterns that would have been difficult to observe from field or standard remote-sensing data. Other applications of the method for the study of intertidal ecosystems are suggested.

## Methods

**Blimp**—We used a 6-m helium-inflated blimp (319 cubic feet; Tern Style). The blimp can lift 6 kg and has been tested by the manufacturer under wind conditions up to  $55 \text{ km h}^{-1}$ . The blimp was controlled from the ground using a tether line attached underneath and onto the front of the blimp. The blimp's altitude was controlled by a storage reel attached to a hand truck, so it could be easily carried along the shore. Two parallel 3-m long nylon lines were fixed under the blimp onto which the camera (*see below*), mounted on a small supporting frame, was attached. This setting allowed the camera to remain horizontal and to stabilize quickly after wind perturbations. At 100-m altitude, camera stability could easily be evaluated from ground by looking at movement of the two parallel nylon lines. The camera was controlled from the ground using an infrared remote control (*see below for details*). The blimp was inflated once, then carried to sampling sites in a 6-m covered van. Inflating the blimp on site for each photography session would have been neither cost nor time efficient due to helium cost and often unsuitable conditions on sampling sites.

**Camera**—We used a Canon EOS-A2 motorized camera (Canon) for this study. This is a standard reflex 35-mm camera, equipped with a Canon 50-mm lens. An infrared receiver attached to the camera (LC-3 Receiver, Canon) allowed triggering from the ground, using an infrared emitter (LC-3 emitter, Canon). The range of the emitter was 100 m, but it could be expanded by attaching an intermediate receiver/emitter module along the tether line. Since 35-mm cameras are not designed for photogrammetric measurements, we calibrated our camera in order to obtain the following parameters: (1) the lens true focal length, which usually differs from the manufacturer setting (i.e., 50 mm), and (2) the precise coordinates of the photo's corner, which do not always form a perfect rectangle. These parameters are necessary for photogrammetric corrections and precise measurements on photos. The focal length was obtained by taking overlapping pictures of a three-dimensional indoor arrangement of surveyed points (Laboratoire de métrologie, Département des sciences géomatiques, Université Laval, Québec, Canada).

Frame coordinates were obtained using a precise stereocomparator (Wild STK1).

**Study site**—Aerial photographs were acquired over a  $325 \times 40 \text{ m}$  long intertidal area, east of Sainte-Flavie, along the South shore of the St. Lawrence estuary (Québec, Canada). The study site was a rocky platform, characterized by a very strong ice disturbance regime, which was dominated by the mussel *Mytilus edulis* and the macroalgae *Fucus* sp. The area photographed was delimited by 36 control points ( $30 \times 30 \text{ cm}$  white panels) anchored onto the bottom. Control points were aligned along two parallel transects, 18 m apart, and parallel to the shoreline. Along each transect, the points were located 18 m apart. Thus, the control points on two transects formed adjacent  $18 \times 18 \text{ m}$  square areas in the midintertidal zone (Fig. 1A). The center of each control point was surveyed precisely using standard survey equipment and mapped ( $X$ ,  $Y$ , and  $Z$  coordinates) in the NAD27 reference system with a precision of 1 cm, using three official geodesic reference points located near the study site (Fig. 1).

**Photography**—Two aerial photography sessions were carried out: one at the beginning (24 May) and the other at the end (6 October) of the 1997 algal growth season. In the first session we characterized topography while the substratum was almost devoid of organisms. In the second session we photographed the community while the biomass of its dominant species was maximum. Photos were taken during clear days, when low-tide period coincided with the sun near zenith. Photographs were taken at an altitude of 80 m (1/1600 scale) in May and 50 m in October, every 6 m, along the center line of control point transects. As the tether line remained vertical, blimp position was controlled by using the ground anchor as the approximate center of photographed areas. Under windy conditions, however, the tether line made an angle that could be measured to determine blimp's altitude and position. This procedure produced sufficient overlapping of photos for photogrammetric analysis and ensured a minimum of four control points on each overlapping section at 80-m altitude. At that altitude the area covered by one photo was  $60 \times 40 \text{ m}$  ( $2,400 \text{ m}^2$ ). With 60% overlap between photos of adjacent areas, each stereoscopic model covered approximately  $1,440 \text{ m}^2$ . We used Fuji Velvia 50 (Fuji Photo) and Kodak Ektachrome 64 (Eastman Kodak) 35-mm professional transparency film in May, and Kodak Ektachrome professional infrared EIR film, with Wratten No. 12 filter in October. Film was kept at  $-18^\circ\text{C}$  before photography and later before processing. For all photos, the focus was set to infinity. EIR film required an exposure index of 200, diaphragm opening of F16, and a speed of 1/30 s. For color transparency film, diaphragm opening and speed were automatically set by the camera.

**Biological calibration**—The benthic community was sampled using  $25 \times 25 \text{ cm}$  quadrats within the photographed area, just after photos were taken on 6 October. Pilot studies showed that having the quadrats placed within the sampling areas during aerial photography created unwanted shading and interference on photos; therefore location of quadrats at the four corners of six control points ( $n = 22$ ; Fig. 3C) are

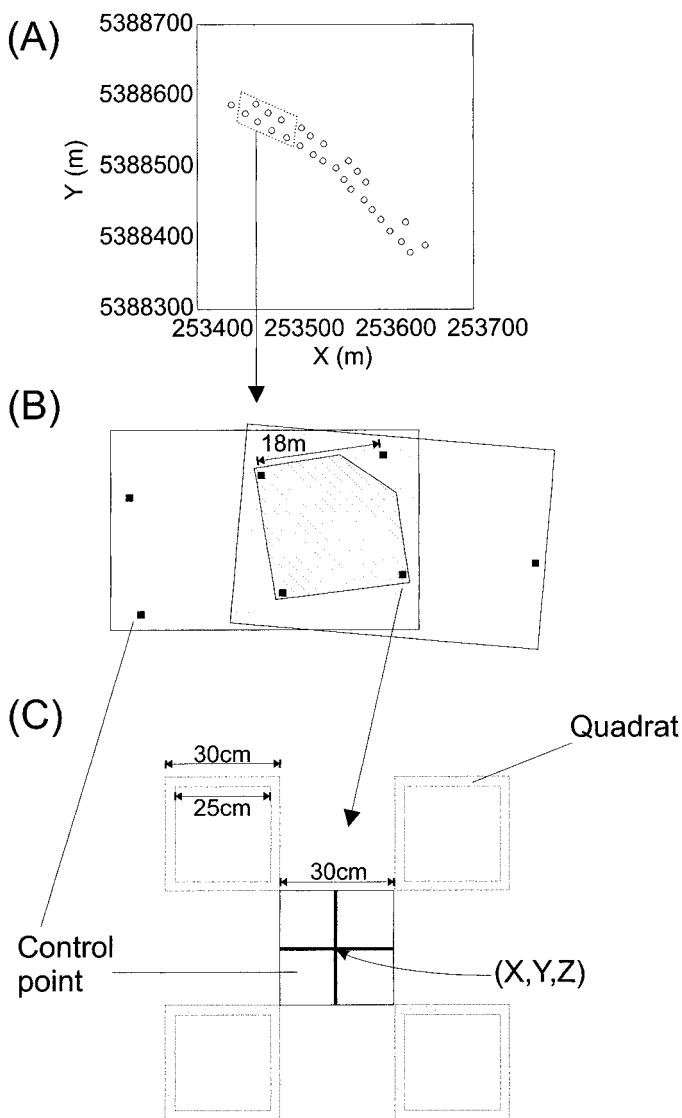


Fig. 1. Control point distribution over (A) the study area and (B) one stereo model used for method validation. Darkened area on (B) shows overlapping area that constitutes one stereomodel (see text for detail) and dashed area illustrates analyzed area where topography was restituted and where *Fucus* biomass was mapped from one red-infrared image. (C) Detail of one control point showing position of biological calibration quadrats.

not shown on photos. Percent cover of *Fucus* sp. was evaluated within each quadrat, and all organisms were removed. Although the corners of six control points (24 points) were identified for biological sampling, only 22 quadrats were actually sampled because of time restrictions. For each sample, all organisms were identified in the laboratory. Each species was freshly weighed after blotting excess water.

### Analysis

**Image scanning**—Film was digitized in 24 bits (red green blue [RGB] colors), at an optical resolution of 2116 dpi, and saved in TIFF format. For photographs taken from an 80-m

Table 1. Results for relative orientation of two independent stereomodels. See text for parameter description.

	$b_x$ (mm)	$b_y$ (mm)	$b_z$ (mm)	$\Omega$	$\Phi$	$\Upsilon$	SD( $\Delta$ )
Model 1	5.64	3.45	-0.16	-0.98	1.79	6.07	0.006
Model 2	5.21	1.1	-0.2	0.15	0.42	-2.94	0.001

altitude, one pixel corresponds to 1.9 cm on the ground. At 50 m (color-infrared photos), one pixel corresponds to 1 cm on the ground.

**Camera calibration**—Focal length of the camera was determined using Bundle software (University of Calgary, Canada). This software takes parameters from stereomodel as determined by DVP (Digital Video Plotter) software (see below) as input data to compute focal length.

**Topography restitution**—Photograph rectification for three-dimensional modeling was performed using DVP software (DVP; Gagnon et al. 1995). Photo rectification was carried out using two pairs of photographs (two photos for model 1 and two photos for model 2, Tables 1 and 2) in order to look at success of rectification on two stereomodels. Rectification was performed with and without camera calibration, in order to evaluate the importance of 35-mm camera calibration for high-resolution remote sensing. The software went through three steps in order to produce the stereomodel: interior, relative, and absolute orientations. While performing interior orientation, the software took some calibrated camera parameters (frame corners coordinates) to compute orthogonal transformation. During relative orientation, we identified six points (5 degrees of freedom + 1 to calculate residuals) on both images to remove the  $y$  parallax ( $py$ ) on these points. The parallax  $x$  is the apparent position change of an object between images due to difference of depth, and the parallax  $y$  is caused by the fact that photographs were not on the same plane. This step allowed us to determine the three components of the model base and the three angles ( $\omega$ ,  $\phi$ ,  $\kappa$ ) defining the relative spatial position of the images. Finally, the software accepted surveyed coordinates of control points to determine absolute orientation. Orientations were then completed, both images appeared side by side on the screen and could be viewed in stereo using a mirror stereoscope (Université Laval, Québec, Canada) mounted on a computer screen. The DVP software allowed users to move a three-dimensional cursor into the model in  $X$ ,  $Y$ , and  $Z$  giving the three coordinates of any point in contact with the cursor. Topographic restitution was performed using a mirror stereoscope and by moving the cursor on the substratum's surface seen in three-dimensional recording. This procedure could be repeated at any location over the overlapping portion of rectified photos.

**Resolution and precision**—Theoretically, resolution is equal to half the pixel size =  $0.01$  m in ( $x$ ,  $y$ ), and to  $0.01f/b$  (where  $f$  is the focal length of the camera and  $b$  the model base  $b_x$  if  $b_y$  and  $b_z$  are negligible, or  $\sqrt{b_x^2 + b_y^2 + b_z^2}$  if they are not) in  $z$ . However, actual resolution is limited by

Table 2. Results for absolute orientation of two independent stereomodels. See text for parameter description.

Reference point	X (m)	$\Delta X$ (m)	Y (m)	$\Delta Y$ (m)	Z (m)	$\Delta Z$ (m)
Model 1						
1	253 559.77	-0.03	5 388 483.71	-0.02	1.62	-0.05
2	253 574.22	-0.03	5 388 494.62	0.02	1.35	0.05
3	253 564.89	0.02	5 388 509.64	0.03	1.51	-0.06
4	253 551.9	0.02	5 388 499.76	-0.04	1.36	0.06
SD		0.03		0.03		0.06
Model 2						
1	253 511.92	0	5 388 531.05	0	1.31	-0.02
2	253 523.67	-0.04	5 388 544.13	0.01	1.3	0
3	253 497.99	0.02	5 388 541.31	-0.04	1.67	0.04
4	253 481.14	-0.01	5 388 552.24	0.03	1.93	-0.02
5	253 515.29	0.03	5 388 542.51	0.01	—	—
SD		0.03		0.02		0.02

errors on all other measurements (ground truthing, image pointing during rectification, film deformation, etc.). We used the standard deviation of differences between pointed and surveyed control point coordinates as an estimate of topographic error along each axis. This parameter was computed by the DVP software for each stereomodel during computation of absolute orientation.

*Image processing for biological calibration*—Photosynthetic plants are known to reflect near-infrared light and to absorb red light (see Lillesand and Kiefer 1994 for a review). Ben Moussa et al. (1989) further showed that reflectance intensity could be related to macroalgae in the intertidal. Lavoie et al. (1990) showed, using a multispectral radiometer, that intertidal *Fucus* biomass in the St. Lawrence Estuary had a maximum correlation with spectral intensity at wavelength centered around 840 nm. The infrared film used has a near-infrared sensitivity between 700 and 900 nm (Eastman Kodak), thus allowing it to detect *Fucus* biomass variations. More precisely, the RGB channels of digitized color-infrared photographs taken in October were used to compute a normalized vegetation index (NDVI; Goward et al. 1991; Lillesand and Kiefer 1994) as  $NDVI = (\text{red} - \text{green}) / (\text{red} + \text{green})$ . The NDVI index varies between -1 and +1. On color-infrared film digitized in RGB channels, the red channel corresponds to near-infrared signal (700–900 nm), and the green channel corresponds to red signal (500–700 nm; Eastman Kodak). We also used the simple ratio (SR) index (Law and Waring 1994) as an index of algal biomass:  $SR = \text{red}/\text{green}$ . This index varies between 0 and 1. Both indices take advantage of the absorbance of red and reflectance of near-infrared wavelengths by vegetation, but reflectance per se was not measured since no radiometrical calibration was carried out and values are thus not intended for comparison with other studies. Index values for each quadrat were computed as the mean of individual pixel index values within image areas corresponding to sampled quadrats in the field. Sampled areas were located and extracted from digitized photographs using Corel® PhotoPaint™ 7.0 software (Corel), converted to color channel specific matrix

format, and analyzed using Mathematica® 3.0 software (Wolfram Research). Each sampled area contained from 529 to 729 pixels. We performed nonlinear regression analysis with the NDVI and SR indices as independent variables and *Fucus* sp. biomass in quadrats as the dependent variable, using the SAS statistical package (SAS Institute). As each quadrat was visible on more than one photo, we averaged each index across all images for each quadrat (1–3) before analysis. We also performed analysis using one photo per quadrat (total of three photos), selecting them to minimize the number of photos needed to cover the whole sampling area.

*Spatial analysis*—Topography restitution was carried out over a regular grid within an area delimited by the four control points visible on stereomodel 2 (18 × 18 m; Fig. 1B, dashed area). Data were recorded at 0.2-m intervals on the ground. We computed the NDVI index and applied the calibration equation (see Results) on each 20 × 20 pixel section over one color-infrared photo covering the same area (Fig. 1B and Fig. 1). Negative NDVI values were set to 0 prior to biomass computation. We thus obtained two raster layers, one for topography, the other for algal biomass, both with 0.2-m pixels on the ground. Spatial offset between topographic and NDVI grids was corrected by linear interpolation on topographic data using Surfer software (Golden Software) in order to obtain one elevation point in the center of each NDVI cell. We produced 10 spatially averaged data sets for each variable by progressively increasing pixel size to 2 × 2 m, by 0.2 m step size. We also generated a raster map of local topographic heterogeneity at each resolution by computing the standard deviation of Z among the eight neighbors of each cell (Moore neighborhood; Durrett and Levin 1994). Substratum type can be linked with elevation as fine sediments are more often found in lower, protected area than on higher and exposed surfaces. In order to quantify the relationship between elevation (Z) and the cover of soft substratum, we divided the analyzed area onto three elevation categories ( $Z < 1.3$  m,  $1.3 < Z < 1.6$  m,  $Z > 1.6$  m) using the least-square fit to draw the elevation contour on the digitized image. We then overlay a 1-m mesh size

grid over the digitized image and determined the number of cells covered by soft substratum for each elevation category. Soft substratum was identified by visual photo interpretation and defined as 60% of a 1-m cell being covered by sediment particle <0.2 m.

We determined the spatial structure of topography and algal biomass by computing semivariograms (Rossi et al. 1992) on both variables individually. Cross-semivariograms were computed between topography and *Fucus* sp. biomass in order to determine scale of maximum correlation between these variables. Geostatistical analysis was performed using Variowin software (Pannatier 1996). For each variable, directional semivariance was computed along two directions: (1) along the north-south axis corresponding to elevation gradient over the analyzed area and (2) along the east-west axis, parallel to the shore (see Fig. 5). In order to determine how spatial averaging affects our interpretation of patterns, we computed squared semipartial correlation coefficients from nonlinear multivariate regression models with algal biomass as the dependent variable and Z and local topographic heterogeneity [SD(Z)] as independent variables, at each resolution level.

## Results

*Time and cost efficiency of the method*—Installing and positioning control points required two low-tide periods (8 h). Photography acquisition sessions were performed by one person along the 325-m long transect and required one low-tide period in May. The October session was also carried out within one low-tide period but covered only a portion of the transect (120 m) since quadrat sampling for biological calibration had to be carried out during the same low tide. Among image-processing steps (see Analysis) only topography restitution was time consuming, requiring 3 s per point. It took 3 d to complete topography restitution presented here.

The total cost of material (blimp, camera and lens, emitter-receiver system) was about the same as the cost for one photo transect carried out using traditional aerial photography techniques (i.e., airborne aerial photography). Each photography session (color and red-infrared photo acquisition over the 325-m long transect) involved costs for helium, film and film processing, and truck rental, which represented about 15% of total equipment cost.

*Camera calibration and stereorectification*—The calibrated focal length was 51.2 mm ( $\pm 0.2$ ). Tables 1 and 2 show results for relative and absolute orientations for each stereomodel. Standard deviation of the difference between surveyed and pointed positions of control points varied from 2 to 6 cm. Using the averaged difference as an estimate of topographic measurement error, we obtained an error of  $\pm 0.03$  m along the X axis,  $\pm 0.03$  and  $\pm 0.02$  m along the Y axis, and  $\pm 0.06$  and  $\pm 0.02$  m along the Z axis, for the stereomodels 1 and 2, respectively. By comparison, the stereomodel without calibration data for the camera was obtained with a error of  $\pm 0.25$  m along the Z axis.

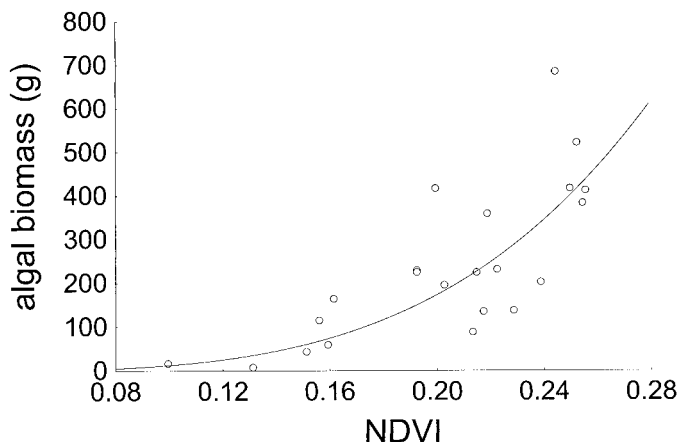


Fig. 2. Power regression model fitted to the relationship between NDVI and algal biomass in quadrats (biomass =  $7.57 \times 10^4 \times \text{NDVI}^{3.78}$ ,  $R^2 = 0.73$ ,  $n = 22$ ,  $p < 0.01$ ).

*Biological calibration*—A large proportion of algal biomass variability (73%) among quadrats was explained by NDVI computed on aerial photos. NDVI estimated over the same quadrat from different photos had a mean variability of 7% (Coefficient of variation). This relationship between NDVI and algal biomass was best described by a power (i.e., log-log linear) function (Biomass =  $121.176 \text{NDVI}^{3.778}$ ,  $n = 22$ ,  $p < 0.001$ ; Fig. 2). The power function fitted to NDVI computed from a single image per quadrat (see Analysis) gave a similar coefficient of determination of 74.4%. The same regression model with the SR index explained 70% of algal biomass variability. The NDVI index in sampled quadrats varied from 0.10 to 0.26 and produced a biomass calibration range of 0 to  $1.12 \text{ g cm}^{-2}$ .

*Topographic and algal biomass restitution*—Figure 3 shows an example of the digitized grayscale images used for photogrammetric analysis. Figure 4 shows topography ( $\pm 0.02$  m) in May 1997 and algal biomass ( $\text{g cm}^{-2}$ ) in September 1997 of the area over which topography restitution was carried out using DVP software. Elevation above zero level varied from 0.77 to 2.27 m and the NDVI index varied from 0 to 0.61, with algal biomass derived from the NDVI index using the calibration equation varying from 0 to  $15.1 \text{ g cm}^{-2}$ . Elevation contour lines highlighted major topographic features over the area (Fig. 4), like a  $0.5 \times 0.5$  m concrete experimental cylinder on the left part of the image (see Fig. 3), boulder area along the  $X = 512$  m axis, and the sharp elevation gradient along the  $X = 507$  m axis. Moreover, by comparing the topographic map (Fig. 4) with the grayscale digitized image (Fig. 3), we observed an association between low elevation areas at the scale of the image with soft substratum, whereas higher areas were composed of hard substratum. This association is also highlighted by soft substratum cover as a function of elevation categories. Soft substratum covered 5% of high portion of analyzed area ( $Z > 1.6$  m), 29% of intermediate elevation area ( $1.3 < Z < 1.6$  m), and 32% of low area ( $Z < 1.3$  m). *Fucus* algae are rockweed, absent from soft substratum areas (Norton 1984) and unable to settle and colonize unstable

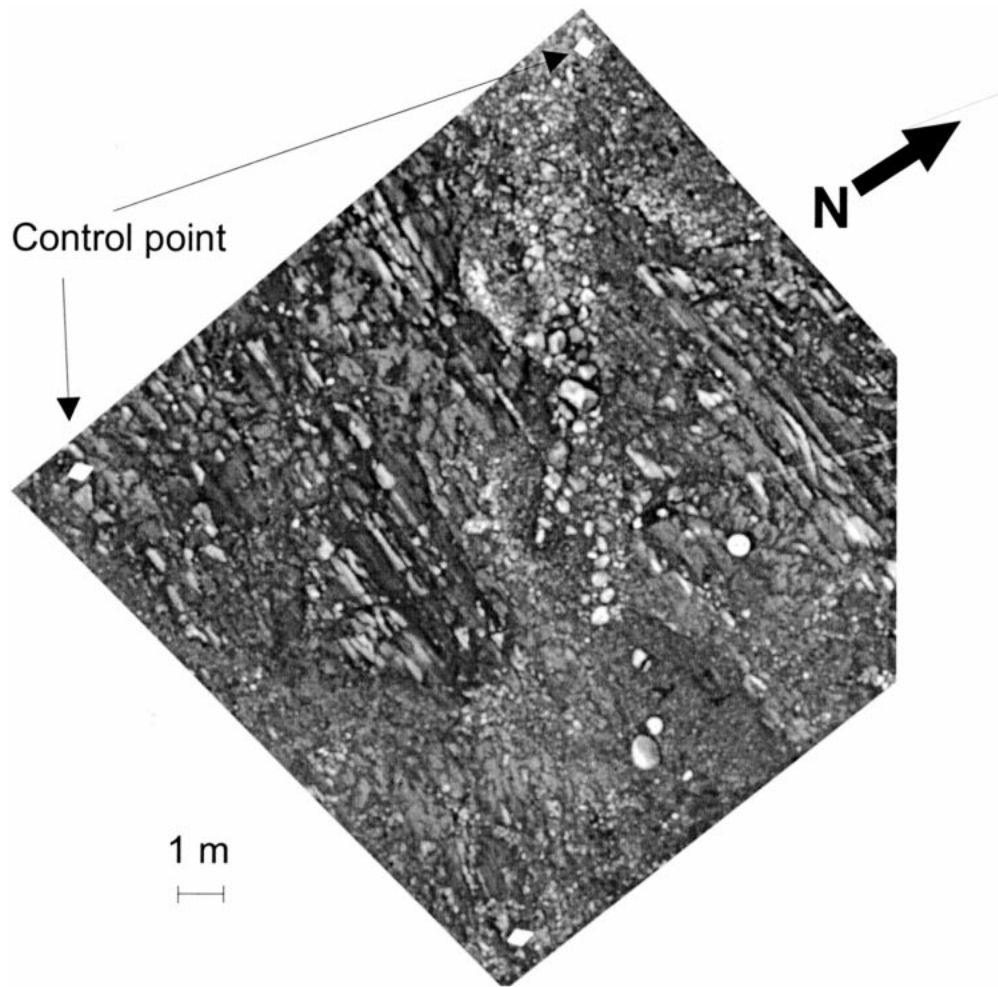


Fig. 3. Digitized image showing the  $18 \times 18$  m analyzed area delimited by control points.

substrata likely to be overturned by wave action (Sousa 1979). After removal of soft substratum areas from the image, we observed a positive relationship between algal biomass and elevation mostly limited to the low intertidal area ( $Z < 1.4$  m; Fig. 5A).

*Spatial analysis*—Semivariogram of elevation revealed anisotropic spatial structure. Figure 6A showed a near linear semivariance curve, revealing an elevational gradient along the axis perpendicular to the shore (north-south axis; see Fig. 3). Along the shore, a steeper spatial dependence structure was observed for  $Z$  over the whole analyzed area, as shown by the Gaussian semivariance pattern (Fig. 6B) with range of 15 m, i.e., about 60% of maximum length of analyzed area (see Fig. 4). Along both directions algal biomass showed spatial dependence up to an initial value of  $8 \text{ g}^2$  (Fig. 6C,D), but this value was reached at a shorter lag in the north-south variogram (4 m, Fig. 6C). However, algal biomass had a more complex spatial structure along the axis parallel to shoreline (east-west axis), showing periodical and hierarchical spatial continuity. The larger scale of periodicity was 8 m as two semivariance peaks were observed at 12 m and a smaller one around 4 m lags. Another scale of peri-

odicity of 2 m could be detected with lower intensity and nested within the 8-m periodicity (Fig. 6D). Comparison between spatial structure of algal biomass along both axes (Fig. 6C,D) also highlights an elongation of patches along the axis parallel to the shore since spatial dependence is observed at larger lags along the east-west than along the north-south axis. Cross-semivariance between algal biomass and  $Z$  along the elevation gradient revealed that algal distribution did not respond to local gradient but were negatively correlated at lags above 8 m. On the other hand, algal biomass and  $Z$  had an increasing correlation between 8 and 14 m. This scale of maximum spatial correlation between elevation and biomass along the east-west axis corresponded to (1) a scale near the range of topographic spatial dependence (Fig. 6B) and (2) a scale at which maximum algal biomass variance was observed (Fig. 6D).

Within a smaller range of scales (0.2–2 m), spatial aggregation influenced the relationship between topography and algal biomass. Figure 7 shows the mean  $R^2$  from a nonlinear multivariate regression model between algal biomass, height above zero level, and local topographic heterogeneity [ $\log(\text{algal biomass}) = aZ^2 + bZ + cSD_{(Z)}^2 + dSD_{(Z)} + e$ ]. For scales inferior to 1.4 m, we performed nine runs of the

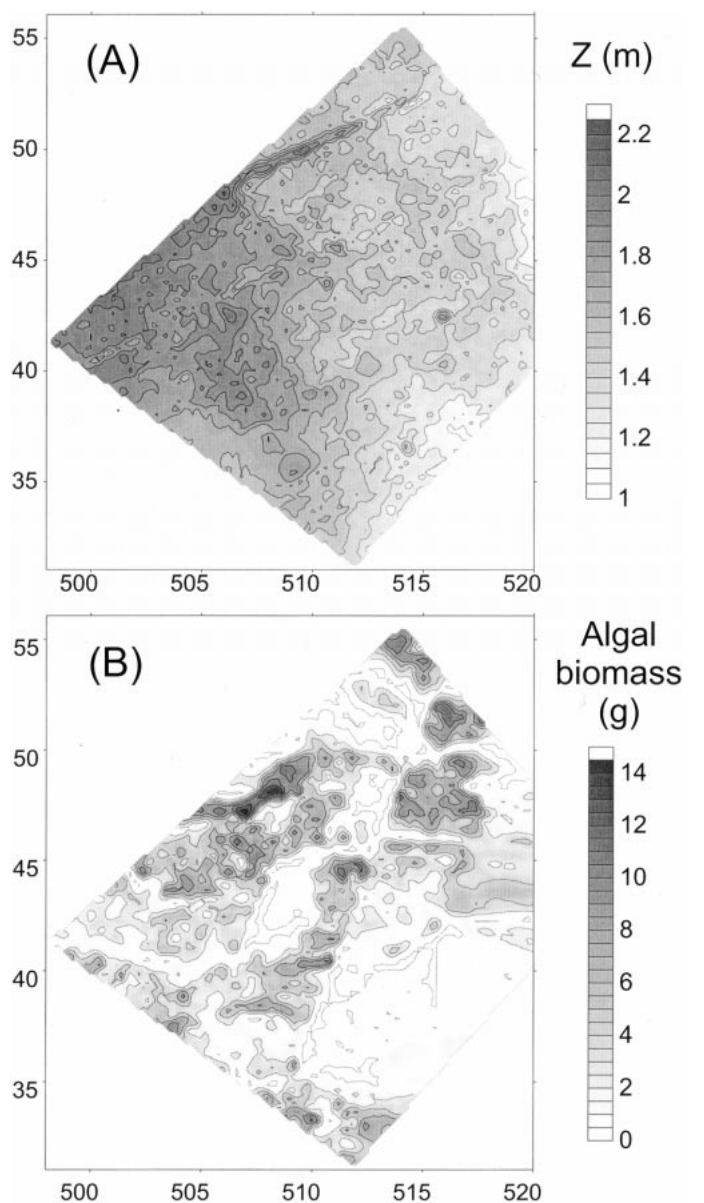


Fig. 4. Contour maps of (A) topography and (B) algal biomass over the  $18 \times 18$  m test area.

regression model, each time by randomly selecting 75 data points in order to control for the change in sample size as a function of spatial aggregation. For larger scales, sample size was less than 75, and we thus performed one run with all data points. Both topographic descriptors explained an increasing proportion of algal biomass variability, from 10% at 0.2 m to 42% at 1.8 m, and correlation strength reached a maximum at 1.8 m, dropping to 17% at 2 m (Fig. 7). The relative importance of each topographic descriptor was also influenced by spatial aggregation. Height above zero level was the most important parameter at scales  $\leq 1.2$  m but was less important than local topographic heterogeneity at higher scales (Fig. 7). Figure 8 shows the influence of topography on algal biomass at 1.8-m resolution [ $\log(\text{algal biomass}) = -4.8Z^2 + 16.6Z + 2917.9SD_{(Z)}^2 - 83.1SD_{(Z)} - 12.9$ ;  $R^2 =$

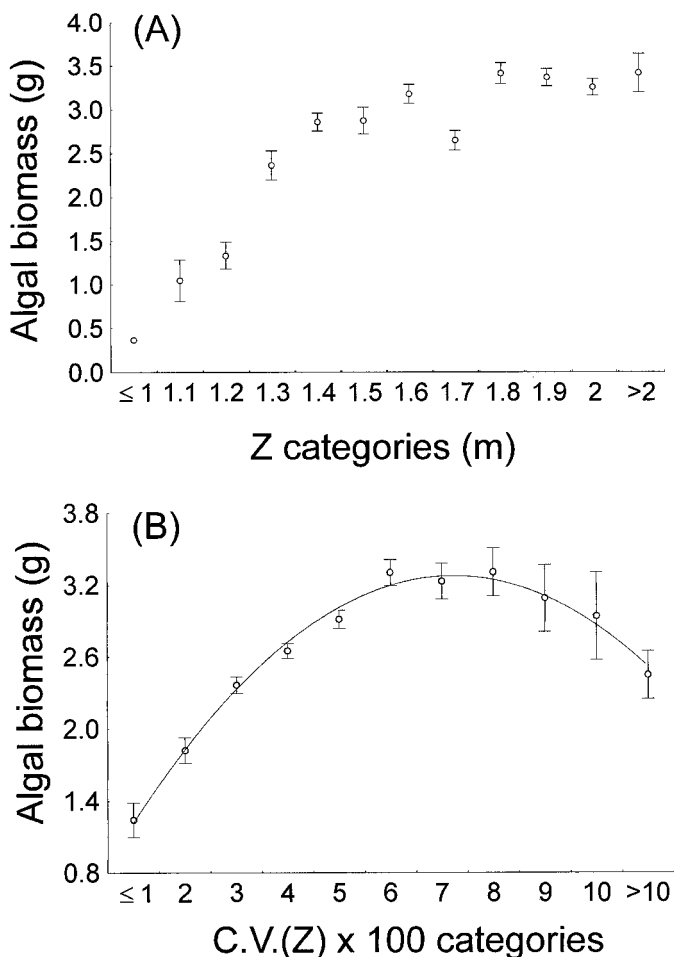


Fig. 5. Influence of (A) hard substratum elevation and (B) topographic variability [CV(Z)] categories on mean algal biomass ( $\pm$ SE) with quadratic regression models fitted to data ( $p < 0.001$ ,  $R^2 = 0.99$ ).

0.43,  $p = 0.019$ ,  $n = 25$ ]. Clustering data into coefficient of variation of Z categories further revealed the general relationship between topography and algal biomass at 0.2-m resolution (Fig. 5B). Small variations of local topographic heterogeneity had a strong positive influence on algal biomass up to C.V. = 6%, then influenced negatively mean algal biomass.

## Discussion

We developed and calibrated a low-cost blimp-based remote-sensing technique and applied this technique to an intertidal ecosystem. From digitized photographs with 0.02-m resolution we were able to derive (1) topographic data with an average error of 0.03 m, and (2) algal biomass data from color-infrared photographs at a resolution of 0.2 m. Seventy-three percent of variability in algal biomass calibration data was explained by the NDVI index computed on digitized color-infrared photographs.

*Topographic restitution*—Topography, and many aspects of topographic variability (slope, drainage, exposition, to-

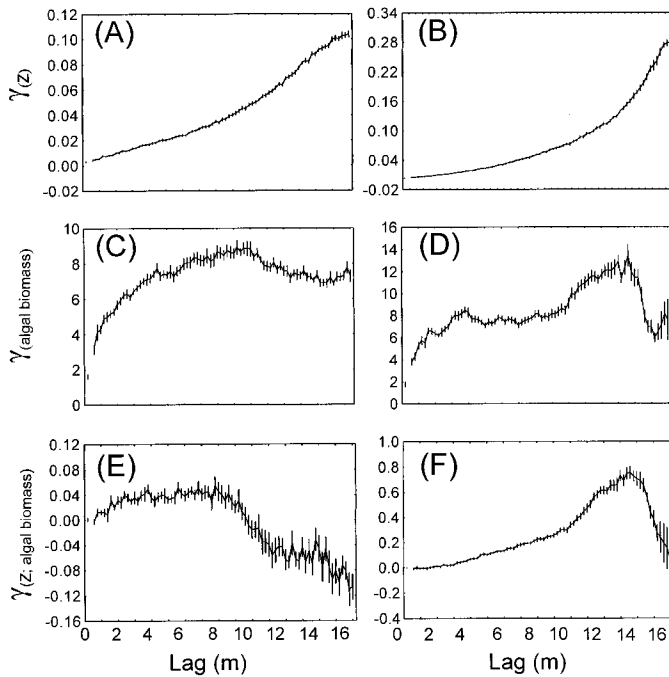


Fig. 6. Variograms along the north-south (A),(C) and the east-west (B),(D) axes for topography (A),(B) and algal biomass (C),(D). Cross-semivariance as a function of spatial lag between topography and algal biomass along the north-south (D) and the east-west (F) axes. Each data point is the average of semivariance values computed from 10 random subsets ( $n = 492$ ) of the whole data set ( $n = 7460$ ).  $\pm$ SE.

pographic complexity) are recognized as major factors explaining spatial structure in marine (Wolanski and Hammer 1988), freshwater (Rasmussen 1988), and terrestrial ecosystems (Takaoka and Sasa 1996). Digital elevation models (DEM) are commonly used to explain ecological spatial patterns from remotely sensed data (Qi and Woo 1996) but are usually derived from field surveys using standard or global positioning system survey equipment. Although the precision of these methods can be very high ( $<0.01$  m), the sampling cost and time associated with field methods usually prevent their use to extensively describe topographic heterogeneity and to perform multiscale analysis below or near the meter scale range over which experiments have tested the local influence of topographic heterogeneity on the structure of intertidal communities (Breitburg et al. 1995; Cusson and Bourget 1997; Guichard and Bourget 1998). Photogrammetric analysis allowing computer topographic restitution is usually performed using expensive calibrated cameras mounted on aircrafts flying at relatively high altitudes ( $>500$  m) (Lillesand and Kiefer 1994). The cost of such techniques limits their use in ecological studies over areas not covered for other purposes. In intertidal ecosystems, the study of topographic heterogeneity relies mostly on coarse DEM (Delafontaine and Flemming 1989) and on local measures of topographic complexity indices in experimental plots (McCormick 1994; Guichard and Bourget 1998). We successfully calibrated a standard 35-mm camera and obtained all parameters necessary to perform high-quality photogram-

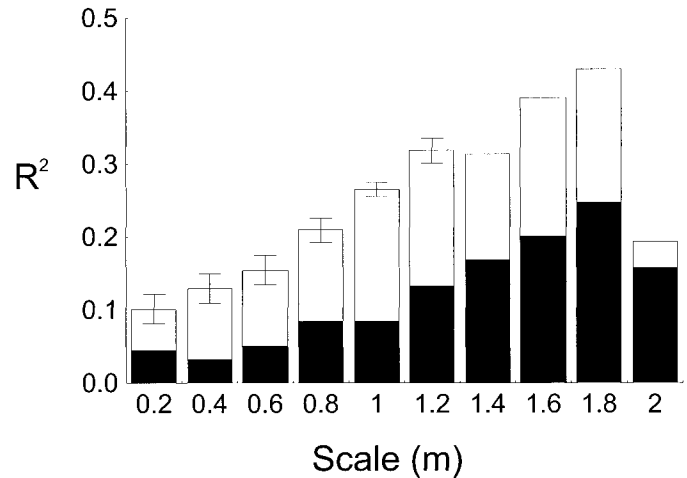


Fig. 7. Total percentage variability in algal biomass ( $R^2$ ) explained by regression models (see Results for details) using elevation and local topographic heterogeneity as independent variables, as a function of aggregation level and expressed as the sum of semipartial correlation coefficients between algal biomass and (1) elevation (white areas) and (2) topographic heterogeneity (black areas).  $\pm$ SE.

metric analysis on overlapping photographs. Using a blimp to carry the camera allowed us to control the altitude precisely from 5 to 100 m, difficult if not impossible to attain with other airborne equipment. At 80-m altitude, digitized photos had a ground resolution of about 0.02 m and topographic restitution was performed with an error of 0.02 m along the Z (elevation) axis. This method required a minimum effort in the field with four control points for each stereomodel ( $40 \times 40$  m). We surveyed 36 control points over a 400-m transect. It would be possible to limit the number of control points to four over a whole transect using

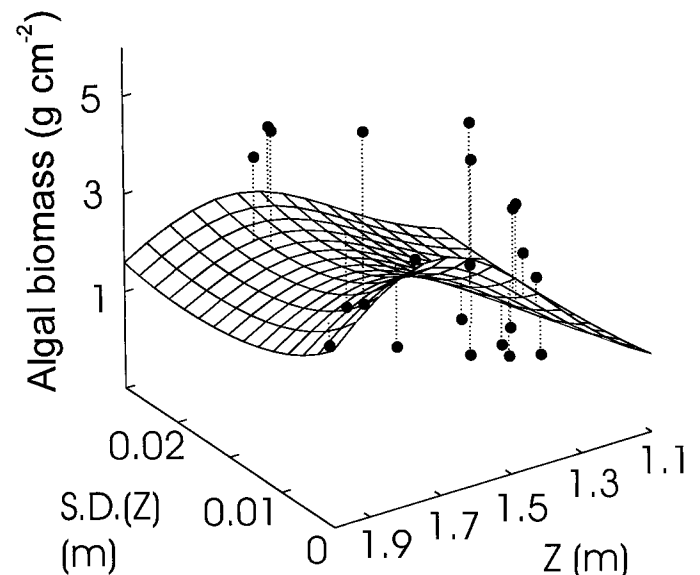


Fig. 8. Regression model (see Results for details) fitted to the relationship between elevation, local topographic heterogeneity [SD(Z)], and algal biomass for data aggregated at 1.8-m resolution.

aerotriangulation techniques, as long as photographs are continuous over the transect. Such techniques could affect spatial precision due to additional image manipulation. The resulting database matched the spatial resolution and extent of algal biomass data.

*Algal biomass estimation*—The normalized difference vegetation index (NDVI) has been used to estimate leaf area index (Badhwar et al. 1986), biomass, and percent cover of vegetation in terrestrial ecosystems, with satellite imagery, airborne (Goward et al. 1991; Sader and Winne 1992), and hand-held (Law and Waring 1994) spectral sensors. NDVI has been used with digitized color-infrared aerial photographs to qualitatively classify and map vegetation cover in terrestrial ecosystems (Jackson and Gaston 1994; Lobo et al. 1998). In coastal habitats, airborne multispectral sensors have been used to assess subtidal seagrass and mangrove cover and biomass at 1-m resolution from bottom (Mumby et al. 1997) index and NDVI (Green et al. 1998). In intertidal ecosystems, Lavoie et al. (1989) used a multispectral sensor to estimate macroalgal biomass at 1-m resolution from near-infrared spectral channels, and the NDVI index was computed from satellite imagery to estimate intertidal macroalgal coverage (Ben Moussa et al. 1989). We computed the NDVI index from digitized 35-mm color-infrared photos and calibrated the index to quantitatively estimate macroalgal biomass at 0.2-m resolution over a  $18 \times 18$  m intertidal area. We were able to estimate algal biomass with 73% accuracy using a regression model. One cause of additional variability for biomass estimation was uncertainty about biomass estimation above the field calibration biomass range ( $>1.12 \text{ g cm}^{-2}$ ). Although calibration data sampled on smooth areas had maximum NDVI values of 0.26 and maximum predicted biomass of  $1.12 \text{ g cm}^{-2}$ , estimated biomass over the study site reached  $15.1 \text{ g cm}^{-2}$ . Algal biomass density ( $>3.3 \text{ g m}^{-2}$ ) has previously been sampled on smooth substratum areas of the study site (Guichard & Bourget 1998), but these values are still inferior to high biomass density found in complex areas such as large crevices formed by large ( $>0.5$  m) boulder aggregates or major substratum complexity, where *Fucus* species formed very dense and thick mats protected from ice disturbance (Bergeron and Bourget 1984). Although our results showed a strong relationship between NDVI and algal biomass, future calibration should be extended to take maximum biomass densities into account. For very high densities where algal canopy forms a thick three-dimensional matrix, temporal topographic data could provide canopy thickness data that could be included in the calibration regression model. Including topographic data during the biomass estimation process could also allow us to control for the influence of slope on reflectance (Colwell 1974). Other improvements of estimation accuracy include prior classification of digitized images using segmentation and discriminant analysis (Lobo 1997), or principal component analysis (Tomer et al. 1997). These methods could help discriminate bare substratum area interfering with photosynthetic reflectance signal (Colwell 1974) and be used to classify the spatial structure of dominant invertebrate species and substratum types.

*Scales of topographic heterogeneity and algal biomass*—

The influence of spatial resolution on remotely sensed pattern interpretation has been described (Qi and Woo 1996), but scaling rules must be drawn from experimental studies of processes involved in scale-dependent pattern formation. In intertidal ecosystems, millimeter-scale topographic heterogeneity has been shown to influence algal settlement (Johnson 1994). At the centimeter scale, crevices have been shown to enhance algal biomass (Archambault and Bourget 1996) by offering protection against ice disturbance (Archambault and Bourget 1983). At the meter scale, limpet grazing patterns were shown to create patchiness in macroalgal distribution at scales  $<2$  m (Johnson et al. 1997), and topographic heterogeneity in the form of natural boulders was shown to influence intertidal community structure (Cusson and Bourget 1997) and more particularly to reduce algal biomass through their influence on local hydrodynamic patterns (Guichard and Bourget 1998). In the latter study, algal biomass was shown to increase with topographic scale from 0.6 to 2.2 m (Guichard and Bourget 1998). In the present study, topography had an increasing influence on algal biomass from scales varying from 0.2 to 2 m. Although theoretical studies showed the importance of determining aggregation scales of nontrivial determinism in spatial population dynamics models (Pascual and Levin 1999), our results suggest that second moment (variance) topographic aggregation at 2 m carries nontrivial information for algal population dynamics. Our results also agree with experimental results presented in Guichard and Bourget (1998), which show a scale-dependent cascade between topographic heterogeneity and algal biomass and suggest a process that can be generalized to the whole intertidal landscape in the area examined. Variograms showed that algal biomass spatial structure involved patchiness independent from elevation gradient, at scales around 2 and 8 m. Cross-variograms also revealed spatial dependence between topography and algal biomass at spatial scales above 8 m. Although algal biomass variograms gave further evidence that important processes responsible for algal pattern formation occur below 4 m (*see aggregation analysis*), the larger scale relationship between elevation and algal biomass could be explained by alternance between soft and hard substrata at the scale of the study site, although further analyses are still required in order to establish this relationship.

Such generalization of experimental studies to natural landscapes across scales required exhaustive spatial data from the scale of experiments to the scale of natural pattern formation that would have been very hard to obtain from field measurements. As these results illustrate the relevance of high-resolution data in order to link experimental and theoretical results in intertidal ecosystems, a more detailed analysis could allow one to describe spatial patterning of the community on the study site.

*Evaluation and future use of the method*—Time and cost efficiency of the method depends mostly on the tradeoff between resolution and the extent of photo acquisition scheme. As one pair of overlapping photos could cover a  $60 \times 40$  m area at 2-cm ground resolution, the use of higher altitude photos or of a lens with smaller focal length could decrease

manipulation time and expenses in cases where lower resolution is satisfactory. On the other hand, monitoring individual behavior or microtopographic features would require the user to restrict covered area. A hierarchical photo acquisition scheme can be adopted where some portions of a large area are covered at higher resolution and the remaining portions are covered using higher (>100 m) altitude photographs.

Limits of this method, as of any remote-sensing method, are linked to three-dimensional properties of some community matrices in marine and terrestrial ecosystems. Detection of hidden biomass and topographic features is often impossible using remote observation methods. However, stereo analysis presented here would allow measurement of bar-substratum elevation after a natural or artificial local disturbance and after recolonization of nearby undisturbed community. Applying this method to subtidal habitats is possible but would be limited by water turbidity, and independent field calibration would have to be performed. Other applications include monitoring of local hydrodynamic patterns using tracers and small drifters. It was also applied to studies of organismal behavior in complex environments through low altitude (<10m) temporal monitoring (Guichard and Bourget, unpubl. data). Low cost and flexibility of the method make it suitable for temporal monitoring of physical and biological patterns.

*Conclusion*—The study of scale-dependent relationships between environmental and biological variables in intertidal ecosystems requires (1) experimental test of scale-dependent processes and (2) multiscale analysis of natural patterns with sufficient resolution to establish the link between patterns and processes. We presented a remote-sensing method able to provide high-quality and high-resolution spatiotemporal data about a key environmental variable (i.e., topography) and algal biomass. Spatial analysis performed on these data revealed patterns that matched experimental evidence showing a scale-dependent relationship between local topographic variability and algal biomass. Although other remote-sensing methods were available, no other approach was able to cover the range of spatial scales of interest. The remote-sensing method presented here will also permit spatial classification of intertidal communities and low-cost temporal monitoring of spatial patterns that could be coupled to spatially explicit models of intertidal population dynamics in complex environments.

## References

- ARCHAMBAULT, D., AND E. BOURGET. 1983. Importance du régime de dénudation sur la structure et la succession des communautés intertidales de substrat rocheux en milieu subarctique. *Can. J. Fish. Aquat. Sci.* **40**: 1278–1292.
- ARCHAMBAULT, P., AND E. BOURGET. 1996. Scales of coastal heterogeneity and benthic intertidal species richness, diversity and abundance. *Mar. Ecol. Prog. Ser.* **136**: 111–121.
- BADHAWAR, G. D., R. D. MACDONALD, AND N. C. MEHTA. 1986. Satellite-derived leaf-area-index and vegetation maps as input to global carbon cycle models: A hierarchical approach. *Int. J. Remote Sens.* **7**: 265–281.
- BAJOUK, T., J. POPULUS, AND B. GUILLAUMONT. 1998. Quantification of subpixel cover fractions using principal component analysis and a linear programming method application to the coastal zone of Roscoff (France). *Remote Sens. Environ.* **64**: 153–165.
- BEN MOUSSA, H., M. VIOLLIER, AND T. BELSHER. 1989. Télédétection des algues macrophytes de l'Archipel de Molène (France) radiométrie de terrain et application aux données du satellite SPOT. *Int. J. Remote Sens.* **10**: 53–69.
- BERGERON, P., AND E. BOURGET. 1984. Effet du froid et des glaces sur les peuplements intertidaux des régions nordiques particulièrement dans l'estuaire du Saint-Laurent. *Océanis* **10**: 279–304.
- BIJLSMA, R. J. 1993. The characterization of natural vegetation using first-order and texture measurements in digitized, color-infrared photography. *Int. J. Remote Sens.* **14**: 1547–1562.
- BOOSE, E. R., D. R. FOSTER, AND M. FLUET. 1994. Hurricane impacts to tropical and temperate forest landscapes. *Ecol. Monogr.* **64**: 369–400.
- BREITBURG, D. L., M. A. PALMER, AND T. LOHER. 1995. Larval distributions and the spatial patterns of settlement of an oyster reef fish: Responses to flow and structure. *Mar. Ecol. Prog. Ser.* **125**: 45–60.
- CARPENTER, R. C., AND S. L. WILLIAMS. 1993. Effect of algal turf canopy height and microscale substratum topography on profiles of flow speed in a coral-reef environment. *Limnol. Oceanogr.* **38**: 687–694.
- COLWELL, J. E. 1974. Vegetation canopy reflectance. *Remote Sens. Environ.* **3**: 175–183.
- COULSON, M. G., J. T. C. BUDD, R. G. WITHER, AND D. J. NICHOLLS. 1980. Remote sensing and field sampling of mudflat organisms in Langstone and Chichester Harbours, Southern England. *In* J. H. Price, D. E. G. Irvine, and W. F. Farnham [eds.], *The shore environment I. Methods*. Academic.
- CUSSON, M., AND E. BOURGET. 1997. Influence of topographic heterogeneity and spatial scales on the structure of the neighboring intertidal endobenthic macrofaunal community. *Mar. Ecol. Prog. Ser.* **150**: 181–193.
- DELAFONTAINE, M. T., AND B. W. FLEMMING. 1989. Effect of larvae settlement, topography and wave action on the establishment of the intertidal barnacle *Tetraclita serrata* Darwin, p. 363–371. *In* J. S. Ryland and P. A. Tyler [eds.], *Reproduction, genetics and distributions of marine organisms*. 23rd European Marine Biology Symposium. Olsen & Olsen.
- DEYSHER, L. E. 1993. Evaluation of remote sensing techniques for monitoring giant kelp populations. *Hydrobiologia* **260/261**: 307–312.
- DURRET, R., AND S. A. LEVIN. 1994. Stochastic spatial models: A user's guide to ecological applications. *Philos. Trans. R. Soc. Lond.* **343**: 329–350.
- GAGNON, P., M. BOULIANNE, J. AGNARD, AND C. NOLETTE. 1995. Present status of the DVP system. *Geomatica* **49**: 479–487.
- GOWARD, S., B. MARKHAM, D. DYE, W. DULANEY, AND J. YANG. 1991. Normalized difference vegetation index measurements from the advanced very high resolution radiometer. *Remote Sens. Environ.* **35**: 257–277.
- GREEN, E. P., P. J. MUMBY, A. J. EDWARDS, C. D. CLARK, AND A. C. ELLIS. 1998. The assessment of mangrove areas using high resolution multispectral airborne imagery. *J. Coast. Res.* **14**: 433–443.
- GUICHARD, F., AND E. BOURGET. 1998. Topographic heterogeneity, hydrodynamics, and benthic community structure: A scale-dependent cascade. *Mar. Ecol. Prog. Ser.* **171**: 59–70.
- GUILLAUMONT, B., L. CALLENS, AND P. DION. 1993. Spatial distribution and quantification of *Fucus* species and *Ascophyllum nodosum* beds in intertidal zones using spot imagery. *Hydrobiologia* **260/261**: 297–305.
- JACKSON, P. L., AND G. G. GASTON. 1994. Digital enhancement as

- an aid to detecting patterns of vegetation stress using medium-scale aerial photography. *Int. J. Remote Sens.* **15**: 1009–1018.
- JOHNSON, G. L., AND C. L. HANSON. 1995. Topographic and atmospheric influences on precipitation variability over a mountainous watershed. *J. Appl. Meteorol.* **34**: 68–87.
- JOHNSON, L. E. 1994. Enhanced settlement on microtopographical high points by the intertidal red alga *Halosaccion glandiforme*. *Limnol. Oceanogr.* **39**: 1893–1902.
- JOHNSON, M. P., M. T. BURROWS, R. J. HARTNOLL, AND S. J. HAWKINS. 1997. Spatial structure on moderately exposed rocky shores: Patch scales and the interactions between limpets and algae. *Mar. Ecol. Prog. Ser.* **160**: 209–215.
- LAVOIE, A., J.-M. M. DUBOIS, M. GRENIER, AND F. BOIVIN. 1990. Inventaire des ressources en fucales sur la rive sud de l'Estuaire du Saint-Laurent avec le MEIS-II: Premiers résultats. Sherbrooke, CARTEL, Univ. Sherbrooke.
- LAW, B. E., AND R. H. WARING. 1994. Remote sensing of leaf area index and radiation intercepted by understory vegetation. *Ecol. Appl.* **4**: 272–279.
- LE TOURNEUX, F., AND E. BOURGET. 1988. Importance of physical and biological settlement cues used at different spatial scales by the larvae of *Semibalanus balanoides*. *Mar. Biol.* **97**: 57–66.
- LEVIN, S. A. 1992. The problem of pattern and scale in ecology. *Ecology* **73**: 1943–1967.
- LILLESAND, T. M., AND R. KIEFER. 1994. Remote sensing and image interpretation. Wiley.
- LOBO, A. 1997. Image segmentation and discriminant analysis for the identification of land cover units in ecology. *IEEE Trans. Geosci. Remote Sens.* **35**: 1136–1145.
- , K. MOLONEY, O. CHIC, AND N. CHIARELLO. 1998. Analysis of fine-scale spatial pattern of a grassland from remotely-sensed imagery and field collected data. *Land. Ecol.* **13**: 111–131.
- MCCORMICK, M. I. 1994. Comparison of field methods for measuring surface topography and their associations with a tropical reef fish assemblage. *Mar. Ecol. Prog. Ser.* **112**: 87–96.
- MEULSTEE, C., P. H. NIENHUIS, AND H. T. C. VAN STOKKOM. 1988. Aerial photography for biomass assessment in the intertidal zone. *Int. Remote Sens.* **9**: 1859–1867.
- MUMBY, P. J., E. P. GREEN, A. J. EDWARDS, AND C. D. CLARK. 1997. Measurement of seagrass standing crop using satellite and digital airborne remote sensing. *Mar. Ecol. Prog. Ser.* **159**: 51–60.
- NORTON, T. A. 1984. The zonation of seaweeds on rocky shores, p. 7–21. *In* P. G. Moore, and R. Seed [eds.], *The ecology of rocky coasts*. Hodder and Stoughton.
- PACALA, S. W., C. D. CANHAM, J. SAPONARA, J. A. SILANDER, R. K. KOBE, AND E. RIBBENS. 1996. Forest models defined by field measurements: Estimation, error analysis and dynamics. *Ecol. Monogr.* **66**: 1–43.
- PANNATIER, Y. 1996. Variowin: Software for spatial data analysis in 2D. Springer-Verlag.
- PASCUAL, M., AND S. A. LEVIN. 1999. From individuals to population densities: Searching for the intermediate scale of non-trivial determinism. *Ecology*. **80**: 2225–2236.
- QI, Y., AND J. G. WOO. 1996. Effects of changing spatial-resolution on the results of landscape pattern-analysis using spatial autocorrelation indexes. *Land. Ecol.* **11**: 39–49.
- RASMUSSEN, J. B. 1988. Littoral zoobenthic biomass in lakes, and its relationship to physical, chemical, and trophic factors. *Can. J. Fish. Aquat. Sci.* **45**: 1456–1447.
- ROSSI, R. E., D. J. MULLA, A. G. JOURNEL, AND E. H. FRANZ. 1992. Geostatistical tools for modeling and interpreting ecological spatial dependence. *Ecol. Monogr.* **62**: 277–314.
- ROUGHGARDEN, J., S. W. RUNNING, AND P. A. MATSON. 1991. What does remote sensing do for ecology? *Ecology* **72**: 1918–1922.
- SADER, S. A., AND J. C. WINNE. 1992. RGB-NDVI color composites for visualizing forest change dynamics. *Int. J. Remote Sens.* **13**: 3055–3067.
- SOUSA, W. P. 1979. Disturbance in marine intertidal boulder field: The nonequilibrium maintenance of species diversity. *Ecology* **60**: 1255–1239.
- TAKAOKA, S., AND K. SASA. 1996. Landform effects on fire behavior and postfire regeneration in the mixed forests of northern Japan. *Ecol. Res.* **11**: 339–349.
- TOMER, M., J. ANDERSON, AND J. LAMB. 1997. Assessing corn yield and nitrogen uptake variability with digitized aerial infrared photographs. *Photogramm. Eng. Remote Sens.* **63**: 299–306.
- WOLANSKI, E., AND W. M. HAMMER. 1988. Topographically controlled fronts in the ocean and their biological influence. *Science* **241**: 177–181.

Received: 12 November 1998

Accepted: 17 November 1999

Amended: 29 November 1999